Analytical Methods

ROYAL SOCIETY OF CHEMISTRY

PAPER

View Article Online
View Journal

Cite this: DOI: 10.1039/d5ay01514f

Single-fiber *versus* macroscale electrodes: enzyme loading and impacts on bioelectronic applications in flexible biodevices

Thiago Bertaglia, [a] Daniel S. de Sousa, [a] Rafael N. P. Colombo, [ab] Kamila C. Pagnoncelli, [a] Rodrigo M. Iost, [c] Luana C. I. Faria, [a] Graziela C. Sedenho [a] and Frank N. Crespilho *[a]

The integration of enzymes into miniaturised carbon electrodes is a central challenge in advancing flexible and implantable bioelectronic devices. Here, we investigate how progressive reduction of electrode dimensions, from macro-scale flexible electrodes to single microfiber configurations, affects catalytic performance in the ethanol bioelectrooxidation. Using alcohol dehydrogenase (ADH) as a model enzyme, we show that multi-fiber electrodes maintain high catalytic activity even after substantial size reduction, whereas single-fiber electrodes exhibit a marked decrease in current density and a significant positive shift in the onset potential. These results indicate that the spatial architecture of the electrode strongly influences enzyme loading and electron transfer efficiency. Our study discloses clear performance differences between macro- and micro-scale configurations, showing that the 3D architecture is a crucial factor when designing bioelectrodes. In this regard, our findings contribute to the literature by suggesting that specific immobilization methods are needed in order to produce highly efficient microbioelectrodes.

Received 10th September 2025
Accepted 11th November 2025

DOI: 10.1039/d5ay01514f

rsc.li/methods

1 Introduction

As our lives increasingly depend on electronic devices, the bioelectronic industry has evolved to produce miniaturized devices capable of monitoring various physiological signals, such as blood pressure,[1] respiration rate,[2,3] and biomarkers like lactate[4–6] and cardiac troponin I.[7,8] With the rising demand for reliable power sources for these bioelectronic devices, there remains a gap in technologies that can simultaneously fulfil the requirements of power, biocompatibility, and safety for the end-user. Enzymatic biofuel cells (EBFCs) offer a promising solution for powering bioelectronic devices due to their mild operating conditions, use of highly specific and efficient catalysts, and general safety for the user.[9] Because of these distinctive characteristics, enzymatic biofuel cells have been considered a viable technology to power the next generation of wearable[10,11] and implantable[12] devices. However, their commercialization has been hindered by challenges, including low operating voltages, limited power output and small lifespan.[13,14]

Carbon materials are widespread electrode platforms when manufacturing bioelectrodes for application in EBFCs thanks to their remarkable electrical conductivity and low cost.[15] Carbon-based flexible materials, for instance, are pointed out as valuable platforms for producing both wearable[16,17] and implantable[18,19] devices thanks to their intrinsic flexibility and good biocompatibility. Indeed, an implantable glucose sensor operating *in vivo* was previously reported using glucose oxidase immobilized into a flexible carbon fiber matrix.[18] Fostering enzyme attachment in flexible carbon fibers is usually accomplished by surface modification to achieve a higher content of oxygen-based functionalities which might improve the direct electron transfer rate. For instance, a recent study showed that chemical exfoliation of flexible carbon fibers by using a $KMnO_4$/H_2SO_4 solution preferentially generates beneficial quinone groups on the electrode's surface, leading to an improvement in the bioelectrochemical response of ADH.[20]

Effective enzyme immobilization on bioelectrode surfaces is crucial in developing high-performance biodevices, as it directly impacts the overall bioelectrochemical efficiency. Suboptimal immobilization leads to bioelectrodes with reduced performance, ultimately resulting in EBFCs with lower operational performance.[14] Over recent decades, various immobilization techniques have been developed to improve enzyme retention and performance, including covalent immobilization,[21] physical adsorption,[22] entrapment,[23] and surface affinity.[24] These methods have been employed to produce bioelectrodes and

[a]São Carlos Institute of Chemistry, University of São Paulo, Av. Trabalhador São-carlense, 400, 13566-590, São Carlos, SP, Brazil. E-mail: frankcrespilho@iqsc.usp.br

[b]Department of Chemistry, Federal University of São Carlos, Rodovia Washington Luís s/n km 235, 13565-905, São Carlos, SP, Brazil

[c]Institute of Chemistry, University of São Paulo, Av. Lineu Prestes, 748, 05508-900, São Paulo, SP, Brazil

biofuel cells with enhanced performance and longevity. Nevertheless, integrating enzymes into compact structures, like carbon-based micro and nanoelectrodes, remains a significant challenge that must be addressed to enable high-power, long-lasting micro-biodevices.[25,26] For example, ADH has garnered significant attention in recent years for its ability to efficiently convert ethanol—a renewable and eco-friendly fuel—into acetaldehyde while reducing nicotinamide adenine dinucleotide (NAD^+), which acts as its cofactor. By immobilizing ADH onto a matrix optimized for NADH oxidation, the energy from this reaction can be effectively harnessed.[27]

This study explores the feasibility of using the enzyme entrapment method to fabricate micro-sized ADH-modified bioelectrodes. Four different electrodes were produced in order to investigate the influence of the electrode size on their bioelectrochemical response. The benchmark electrode, henceforward called FCF, was divided into miniaturised electrodes by reducing their weight to half and a quarter, resulting in electrodes named $\frac{1}{2}$FCF and $\frac{1}{4}$FCF. Subsequently, we advanced miniaturization by isolating a single carbon microfiber, creating the s-FCF microelectrode. ADH was then immobilized on each electrode's surface *via* physical adsorption followed by entrapment, and their ethanol bioelectrooxidation performance was evaluated using cyclic voltammetry. The findings reveal that the s-FCF/ADH/Nafion electrode demonstrated lower performance compared to its macrobioelectrode counterparts, underscoring the need for improved immobilization techniques to address the challenge of enzyme integration on micro and nanostructures, such as carbon microfiber electrodes.

2 Materials and methods

2.1. Materials

ADH from *Saccharomyces cerevisiae* (ADH, EC 1.1.1.1, ≥300 units per mg, M_w = 141–151 kDa, lyophilized powder), potassium hexacyanoferrate(II) trihydrate ($K_4[Fe(CN)_6]\cdot 3H_2O$, 99.95%), potassium hexacyanoferrate(III) ($K_3[Fe(CN)_6]$, 99%), ethanol (99.5%) and Nafion®117 aqueous solution (~5% wt) in an aliphatic alcohol mixture were obtained from Sigma-Aldrich®. Potassium permanganate ($KMnO_4$, 99%), potassium chloride (KCl, 99–105%), sodium phosphate monobasic monohydrate ($NaHPO_4\cdot H_2O$, 98–102%), and sodium phosphate dibasic heptahydrate ($NaH_2PO_4\cdot 7H_2O$, 98–102%) were acquired from Synth®. Hydrochloric acid (37%) and sulfuric acid (98%) were purchased from Honeywell Fluka. The polymer acrylonitrile butadiene styrene (ABS) and A. Bond adhesive were sourced from GTMax 3D. NAD^+ (≥95%) and NADH were purchased from Merk®. The fabrication procedure of s-FCF used Scotch tape from 3 M. All chemicals were used as received without further purification otherwise stated elsewhere.

2.2. Fabrication of electrodes and bioelectrodes

The flexible carbon cloth (Delpho Instruments, Brazil) was chemically exfoliated following a previously reported protocol.[28,29] In summary, the chemical exfoliation took place by immersing 0.5 g of the pristine carbon cloth in 20 mmol L^{-1} $KMnO_4$ in 1 mol L^{-1} H_2SO_4, followed by sonication for 3 hours. The removal of exfoliation residues occurred by sequentially rinsing the treated cloth with concentrated hydrochloric acid and distilled water. Afterwards, the exfoliated cloth was dried under vacuum overnight. It is noteworthy that this chemical exfoliation step introduces quinone groups on the surface of the material, which act as mediators and improve the electrooxidation of biomolecules, such as NADH.[28,30]

Four electrode types were fabricated from the exfoliated carbon cloth (Fig. 1a). The benchmark FCF electrode was created by isolating an array of carbon microfibers and defining a fixed geometric area using epoxy resin. This electrode served as a control based on prior successful applications in bioelectrocatalysis within our group. The miniaturization proceeded using a gravimetric approach where the FCF electrode was divided into half and a quarter of its original weight, giving the electrodes $\frac{1}{2}$FCF and $\frac{1}{4}$FCF as a result (Fig. 1a). The smallest electrode, called s-FCF (Fig. 1b), was produced by manually extracting a single carbon microfiber (~6 μm in diameter) from the treated cloth. The electrical contact of the s-FCF electrode comprised either a carbon paste composed of powdered graphite or an array of pristine carbon fibres.

The immobilization of ADH proceeded by incubating FCF, $\frac{1}{2}$FCF, $\frac{1}{4}$FCF and s-FCF in an 8 mg per mL ADH solution at 4 °C for 24 hours, followed by the application of 20 μL of 2.5% Nafion®117 solution at the bioelectrode surface and subsequent drying under vacuum for 10 minutes (Fig. S1). This straightforward methodology was previously employed by our group when preparing bioelectrodes containing glucose oxidase and ADH.[27,31,32] It is noteworthy that the incubation procedure used different strategies for macro and micro-sized electrodes, as the brittleness of s-FCF hindered the application of the ordinary conic-bottomed plastic flasks employed for FCF, $\frac{1}{2}$FCF, and $\frac{1}{4}$FCF. In this regard, a 3D-printed incubator was designed and printed to better accommodate the s-FCF electrode, as we will detail later in the results. Despite using a dedicated 3D printed shape, the ADH immobilization followed the same workflow as its macroelectrode counterparts. In this regard, physical adsorption took place in an 8 mg per mL ADH solution (using the 3D printed shape), followed by entrapment using 10 μL of 2.5% Nafion®117 solution. The amount of Nafion®117 solution employed when immobilising ADH on s-FCF is lower, due to the decreased size of the electrode. The resulting bioanodes were named FCF/ADH/Nafion, $\frac{1}{2}$FCF/ADH/Nafion, $\frac{1}{4}$FCF/ADH/Nafion, and s-FCF/ADH/Nafion according to their respective sizes.

2.3. Microscopic characterization

Surface morphology of the FCF/ADH/Nafion and s-FCF/ADH/Nafion bioanodes was examined using a ZEISS LEO 440 Scanning Electron Microscope (SEM) operating at 15 kV. The samples for SEM analysis consisted of FCF/ADH and s-FCF/ADH prior to the addition of Nafion. This procedure was chosen to allow a direct comparison between the pristine and enzyme-containing surfaces. Topographic analysis was conducted using a Bruker Multimode 8 atomic force microscope.

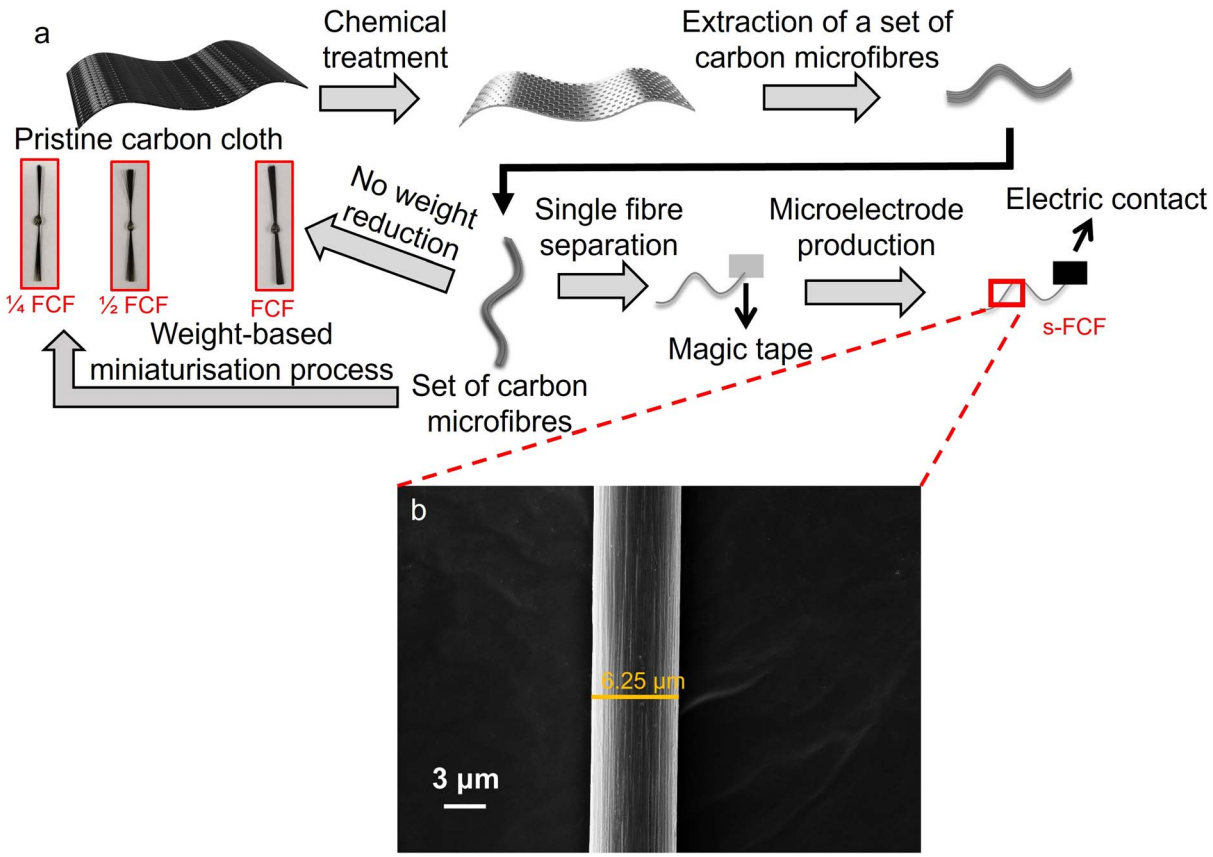

Fig. 1 (a) Schematic of the fabrication process for FCF, ½FCF, ¼FCF, and s-FCF electrodes using a chemically exfoliated flexible carbon cloth. (b) SEM micrograph of a single flexible carbon fibre, with the yellow line indicating the fibre's diameter.

Measurements were taken in intermittent contact mode with antimony-doped silicon tips coated with aluminum (spring constant ~42 N m^{-1}; resonance frequency ~310 kHz). To ensure high topographic fidelity, a scan rate of ≤1 Hz was maintained. Images were processed using second order flattening to remove stage tilt and bow, with no Fast Fourier Transform (FFT) or additional filtering applied during post-processing.

2.4. Electrochemical measurements and enzyme kinetics

All electrochemical measurements were performed by using a μAutolab Type III potentiostat/galvanostat (Metrohm Autolab®, Netherlands) coupled to a three-electrode cell where the (bio)electrodes, a platinum plate, and Ag/AgCl/KClsat served as working, auxiliary, and reference electrodes, respectively. Data acquisition and analysis employed NOVA 2.1.5 software. All electrode potentials reported in this work are referenced to Ag/AgCl/KClsat.

Cyclic voltammetry measurements allowed us to assess the ethanol bioelectrooxidation of the produced bioelectrodes under standardized conditions. All measurements used 0.20 mol L^{-1} phosphate buffer (pH 7.5) containing 0.60 mmol L^{-1} NAD^+ as the electrolyte and the potential was swept from 0.0 to 0.80 V at a 5 mV s^{-1} scan rate. Ethanol was gradually added with a 50% (v/v) ethanol–water stock solution during measurements while monitoring the electrode's electrochemical response. Bioelectrochemical oxidation was continued until saturation, defined as the point where the ethanol oxidation current density showed no further significant change with the ethanol addition. The apparent Michaelis–Menten constant (K_M^{app}) was estimated from a Lineweaver–Burk plot ($1/j$ *vs.* 1/[ethanol]) applied to bioelectrochemical data. The onset potential for ethanol bioelectrocatalysis was determined by drawing a tangent from the background electrochemical response to the recorded cyclic voltammogram (CV). The onset potential is defined as the first point where a clear deviation occurs between the background and the bioelectrocatalytic current. Fig. S2 highlights the onset potential for all electrodes studied. All the electrochemical data obtained were normalised by the electrode area calculated through the Randles–Sevick equation (see Table S1) using the current obtained from CVs recorded in 1.0 mol L^{-1} KCl containing $K_3[Fe(CN)_6]/K_4[Fe(CN)_6]$.

3 Results

3.1. From macro to micro: miniaturizing FCF-based electrodes and bioelectrodes

All electrodes were readily fabricated by handling the flexible carbon cloth, as illustrated in Fig. 1a. The FCF electrode has previously demonstrated successful enzyme immobilization and robust bioelectrochemical performance, making it an ideal benchmark for ethanol bioelectrooxidation in this study.[27,29,30,33]

The $\frac{1}{2}$FCF and $\frac{1}{4}$FCF electrodes were prepared through a gravimetric reduction methodology, reducing the FCF weight to half and a quarter of the original, respectively. The s-FCF electrode comprises a single carbon microfiber, as shown in Fig. 1b, which confirms the effectiveness and simplicity of the separation method. Additionally, Fig. 1b reveals that the carbon microfibers utilized in this study are around 6 μm in diameter, which is consistent with our prior work.[29]

CV using $K_3[Fe(CN)_6]/K_4[Fe(CN)_6]$ as an electrochemical probe highlighted distinct electrochemical behaviours across FCF, $\frac{1}{2}$FCF, $\frac{1}{4}$FCF, and s-FCF electrodes, attributed to their varying dimensions. Fig. 2a shows that the FCF, $\frac{1}{2}$FCF, and $\frac{1}{4}$FCF electrodes exhibit diffusion-limited behaviour with characteristic oxidation and reduction peaks, aligning with the literature. In contrast, the CV of the s-FCF electrode presents a sigmoidal shape with a current plateau, indicative of steady-state currents typical for radial diffusion in microelectrodes (Fig. 2b). This difference arises from the distinct diffusion profiles; while FCF, $\frac{1}{2}$FCF, and $\frac{1}{4}$FCF display semi-infinite diffusion that produces peak-shaped CVs, the s-FCF electrode exhibits radial diffusion, resulting in steady-state currents for both oxidation and reduction reactions. These results confirm that our separation method reliably produces microelectrodes using widely accessible materials.

The application of the Randles–Sevcik equation to raw CVs allowed us to calculate the area of each electrode, as shown in Table S1. The obtained data confirm that the chosen gravimetric miniaturization method influences the available area of the electrodes, as $\frac{1}{2}$FCF and $\frac{1}{4}$FCF have smaller areas than FCF. Also, the area decrease is reasonably proportional to the weight decrease of each electrode, as the area values of $\frac{1}{2}$FCF and $\frac{1}{4}$FCF are 64 and 26% of that obtained for their parent electrode. When comparing the areas of s-FCF and FCF electrodes, one observes that the latter possesses an area 85 times higher than the former. Although the comparison between the electrode weights is not possible in this case, as we could not obtain the weight of a single microfiber using an analytical scale, a visual assessment of the FCF indicates that it consists of a number of microfibers far exceeding 85, as suggested by the area value. A possible explanation for this result relies on the radial diffusion profile of microelectrodes, which provides reactants at a faster rate to the electrode surface, leading to an apparent increase in current. Also, there is the possibility of entanglement among the microfibers inside FCF, which decreases the available area for the electrochemical reaction.

To address the challenge of biomolecule integration on microstructured surfaces, we developed a 3D-printed drawer-based enzyme immobiliser (DBEI) to facilitate enzyme immobilization on microelectrodes (Fig. 2c). The immobiliser comprises three components: the electrode support, the electrode-drawer, and the main body (Fig. 2c). By positioning the microfiber into the electrode support, followed by filling the hole with carbon paste and attaching an array of pristine carbon fibres, one could engineer an easily handleable microelectrode (Fig. 2d). This assembly was later attached to the DBEI's body, which enables the s-FCF to remain immersed in the ADH solution over extended periods (Fig. 2e), enhancing enzyme adsorption. ADH immobilization was achieved *via* physical adsorption followed by Nafion®117 entrapment on all electrodes.

Atomic force microscopy (AFM) micrographs (Fig. 3a–c) illustrate each immobilization step. The oxidatively treated carbon microfibers display surface protrusions due to $KMnO_4/H_2SO_4$ exfoliation, creating a favourable surface for enzyme immobilization (Fig. 3a). The protrusions increase after the incubation of the electrodes in ADH solution, suggesting successful attachment of the enzymes on the electrode's surface (Fig. 3b). The addition of Nafion®117 further smoothens the surface, encapsulating the enzyme within the carbon matrix (Fig. 3c). The kurtosis and roughness data obtained from the micrographs also corroborate these findings as the addition of enzyme leads to an increase in both the Kurtosis and roughness of the electrode followed by a decrease due to addition of Nafion®117 solution (Fig. 3d).

SEM corroborates the success of the chosen enzyme immobilization procedure across electrode scales. The pristine carbon microfiber (Fig. 3e) displays a smooth surface with vertical grooves, which deepen after the chemical exfoliation with $KMnO_4/H_2SO_4$ (Fig. 3f), likely introducing surface defects. Following ADH immobilization, Fig. 3g and h reveal enzyme anchoring on the carbon microfibers, particularly dense in the FCF electrode, as observed in Fig. 3g and S3, suggesting high enzyme loading – a crucial factor for bioelectrode performance. UV-Vis data confirm this, showing a 24-hour enzyme loading of 0.24 mg cm^{-2}, or 1.60 nmol cm^{-2} (see Fig. S4 and Table S2). The s-FCF/ADH/Nafion electrode, however, exhibited lower enzyme attachment due to limited anchoring points on the single microfiber (Fig. 3h and S5). A direct comparison between FCF/ADH and s-FCF/ADH clearly demonstrates the poor enzyme attachment on s-FCF/ADH since the first shows a much higher surface coverage than the latter even at 12× lower magnification. In summary, AFM, SEM and UV-Vis characterization studies show the successful ADH immobilization on the surface of FCF-based electrodes. However, SEM demonstrates the enzyme loading differs from macro to micro-sized electrodes, which could impact the electrochemical response of the microelectrodes.

3.2. The impact of enzyme loading and electrode miniaturization on ethanol bioelectrooxidation

The ethanol bioelectrooxidation by ADH proceeds *via* a bi–bi ordered mechanism, oxidizing ethanol to acetaldehyde while reducing NAD^+ to NADH in the electrolyte.[34] Cyclic voltammetry (Fig. 4a, b and S2) shows ethanol bioelectrooxidation for all bioelectrodes. Interestingly, FCF, $\frac{1}{2}$FCF, and $\frac{1}{4}$FCF electrodes exhibit similar ethanol bioelectrooxidation current densities, with only slight variations in the onset potential (Fig. 4d and S2a–c), suggesting that weight-based miniaturization does not compromise electrode performance. The decrease in the current output (Fig. 4c) probably occurs due to the remarkable decrease in immobilised ADH. While previous work shows the ADH content in an electrode similar to FCF/ADH/Nafion is 0.37 ± 0.07 mg cm^{-2}, the enzyme concentration at $\frac{1}{2}$FCF/ADH/Nafion

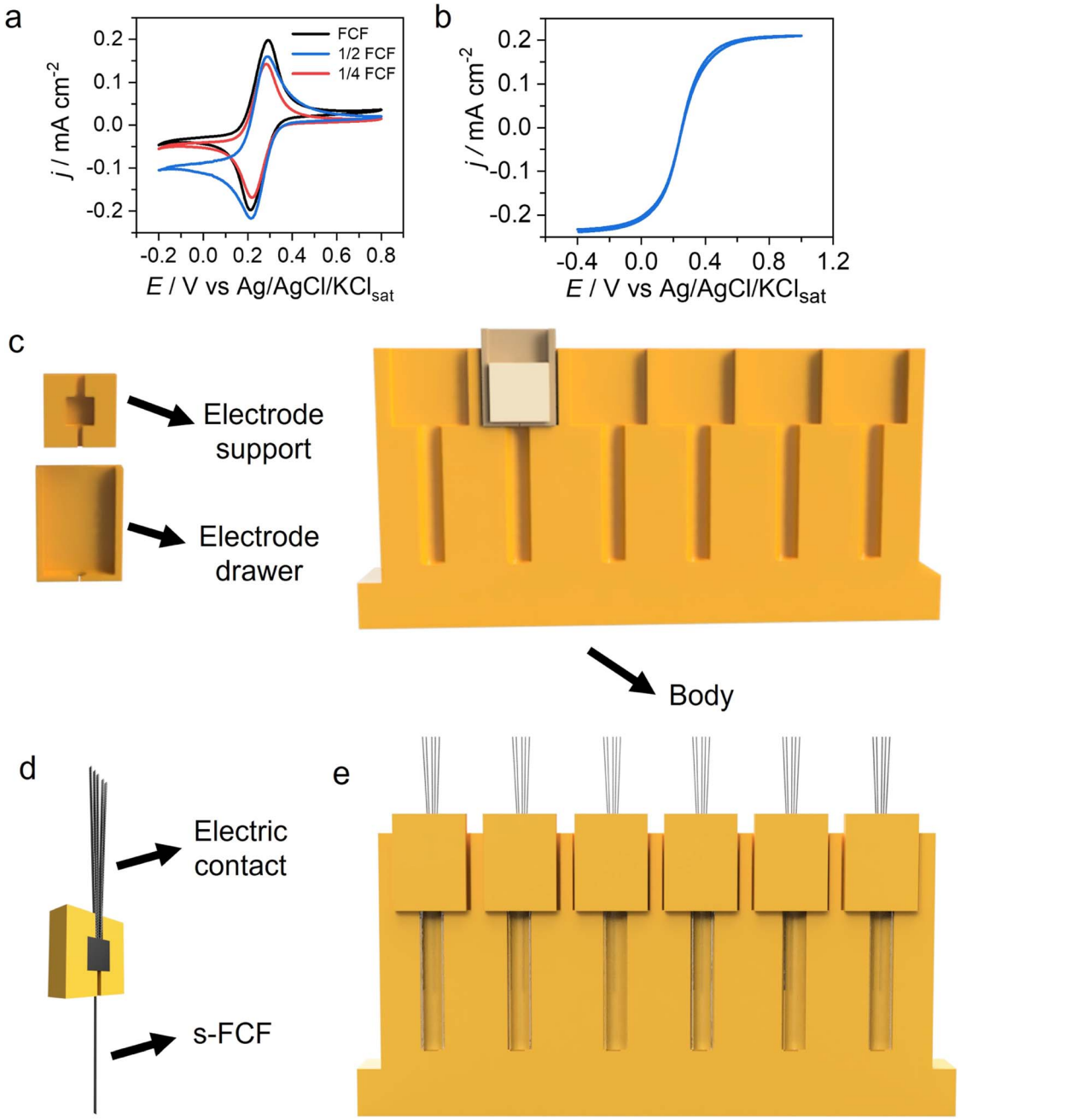

Fig. 2 (a) Cyclic voltammograms (CVs) of FCF, $\frac{1}{2}$FCF, and $\frac{1}{4}$FCF electrodes recorded in a 5 mmol L^{-1} $K_4[Fe(CN)_6]$ solution with 1 mol L^{-1} KCl as the supporting electrolyte. (b) CV of the s-FCF electrode in a 5 mmol L^{-1} $K_3[Fe(CN)_6]/K_4[Fe(CN)_6]$ solution with 1 mol L^{-1} KCl. All CVs were recorded at a scan rate of 5 mV s^{-1} at room temperature. (c) Components of the developed DBEI. The arrows highlight the electrode drawer, the electrode support, and the body. (d) 3D sketch of s-FCF produced using the electrode support and electrode drawer for enzyme immobilization. The electrical contact comprised an array of pristine carbon fibers. (e) ADH immobilization procedure using the DBEI and s-FCF electrodes.

is significantly lower (0.24 ± 0.03 mg cm^{-2}). This direct comparison indicates that the electrode's enzyme content depends on size, corroborating our SEM data, which indicates that s-FCF/ADH has a lower enzyme content than FCF/ADH (Fig. 3g and h). Our electrochemical data suggest the enzyme loading stabilizes from $\frac{1}{2}$FCF/ADH/Nafion to $\frac{1}{4}$FCF/ADH/Nafion, as their current responses are nearly identical. In contrast, the enzyme loading steeply drops for s-FCF/ADH/Nafion as its current response is negligible compared to all macro-bioelectrodes. Thus, the electrochemical results corroborate the previously shown SEM data (see Fig. 3e–h). The probable cause of the poor enzyme immobilization on the s-FCF electrode lies in its 3D structure as it does not have anchoring points for the ADH enzyme to bind, unlike FCF, $\frac{1}{2}$FCF and $\frac{1}{4}$FCF electrodes.

In contrast, the s-FCF/ADH/Nafion shows significantly lower bioelectrooxidation current density compared to FCF/ADH/

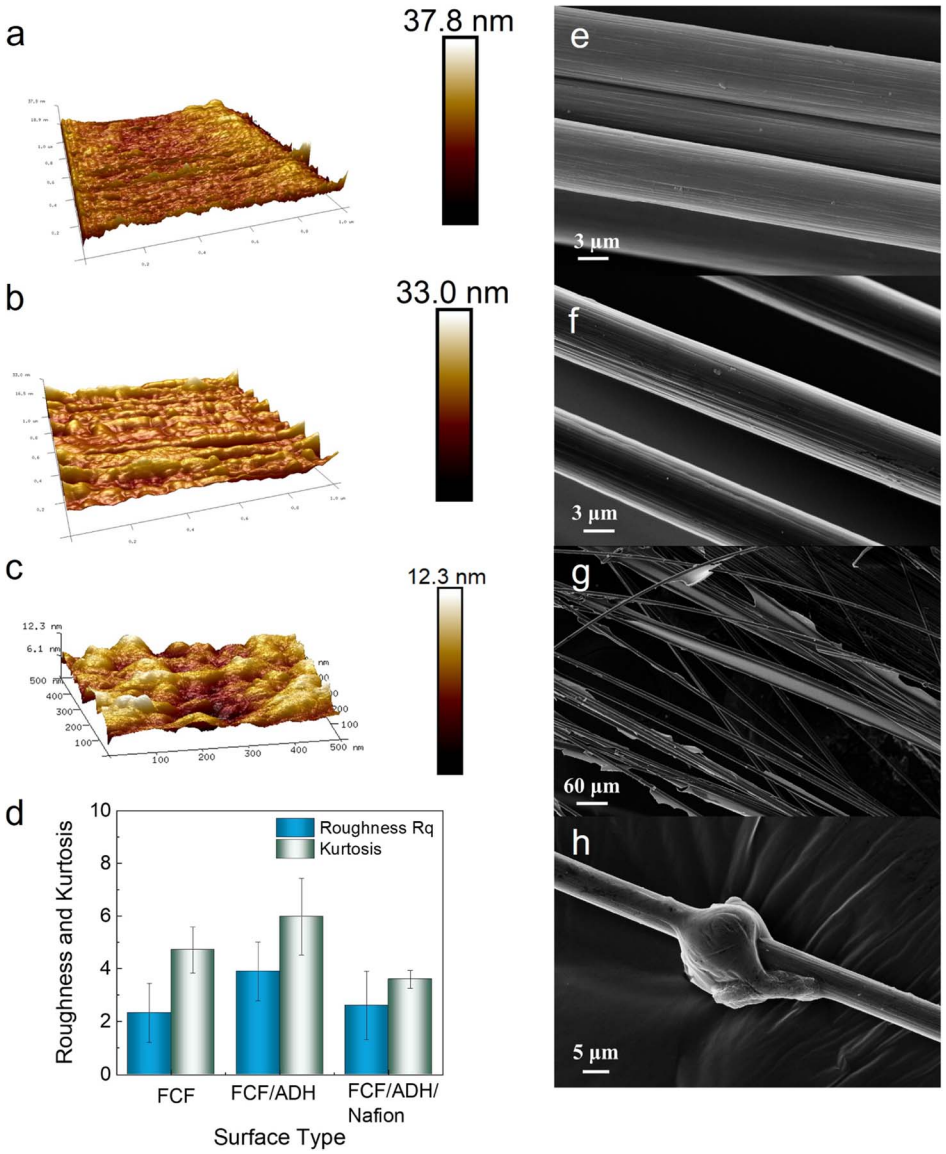

Fig. 3 Atomic force micrograph of (a) FCF before ADH immobilization, (b) FCF after ADH immobilization (FCF/ADH), and (c) FCF/ADH/Nafion bioelectrode. (d) Plot showing the roughness and kurtosis at each stage of ADH immobilization on the FCF surface. Scanning electron microscopy (SEM) images of (e) pristine FCF, (f) chemically exfoliated FCF, (g) FCF/ADH/Nafion, and (h) s-FCF/ADH/Nafion bioelectrodes.

Nafion (Fig. 4b). Surprisingly, the onset potential for ethanol oxidation in s-FCF/ADH/Nafion is shifted by 100 mV to more positive potentials, suggesting much slower kinetics on this microelectrode (Fig. 4d). This onset shift indicates that ethanol bioelectrooxidation at s-FCF/ADH/Nafion requires 19.3 kJ mol^{-1} more energy than at FCF/ADH/Nafion, which may result from poor enzyme attachment on the s-FCF surface.

Previous studies have reported onset potential shifts in bioelectrochemical reactions due to pH,[31] ionic strength variations[35] and enzyme immobilization on pseudocapacitive substrates,[36] such as osmium-based redox polymers. However, the onset shift in microelectrodes is rarely addressed in the literature. We hypothesize that this unusual behaviour occurs due to suboptimal enzyme attachment, which impairs ethanol bioelectrooxidation. To validate this, we examined the onset potential for ethanol bioelectrooxidation on a glassy carbon electrode (GCE) with varying enzyme loadings, ensuring localized ADH immobilization as shown in Fig. 5a. This strategy aims to leave the uncovered carbon framework of GCE facing the electrolyte and consequently observe the impact of poor enzyme immobilization on the bioelectrocatalytic behaviour of GCE. The recorded CVs and onset potentials show that lower enzyme loadings correlate with higher onset potentials, confirming our hypothesis (Fig. 5b–d).

Notably, the GCE with the highest enzyme coverage (563 µg cm^{-2}) shows an onset potential close to that of FCF/ADH/Nafion, underscoring the impact of good enzyme coverage on the ethanol bioelectrooxidation profile of bioelectrodes. Also, this result suggests that the FCF/ADH/Nafion bioelectrode has more homogeneous enzyme coverage, which aligns with our

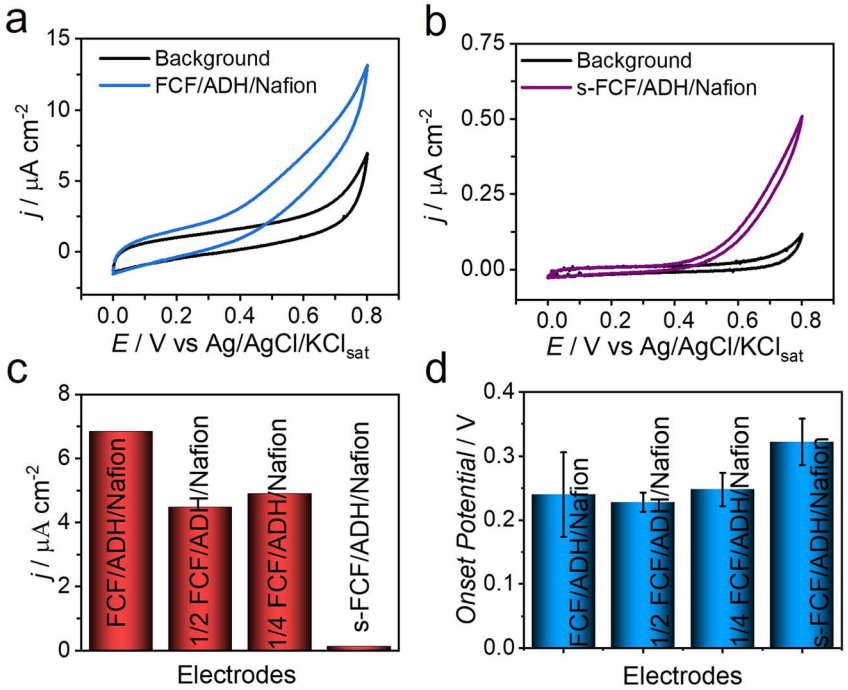

Fig. 4 (a) CV of the FCF/ADH/Nafion bioelectrode in the absence (black) and presence (blue) of 0.25 mol L^{-1} ethanol. (b) CV of the s-FCF/ADH/Nafion bioelectrode in the absence (black) and presence (purple) of 0.085 mol L^{-1} ethanol. Both ethanol bioelectrooxidation studies were conducted in 0.2 mol L^{-1} phosphate buffer (pH 7.5) containing 0.6 mmol L^{-1} NAD^+ as the supporting electrolyte, at a scan rate of 5 mV s^{-1} and room temperature. (c) Comparison of current density at 0.6 V and (d) onset potential for ethanol bioelectrooxidation across all produced bioelectrodes.

previous SEM micrographs as they show a reasonable amount of ADH spread over the microfibers of the FCF electrode. In this regard, from a bioelectrochemical point of view, these results suggest that electrodes containing multifiber arrays are a more suitable platform for the preparation of enzyme-containing bioelectrodes as the microfibers act as anchoring points for the enzymes, boosting the enzyme coverage and loading. Consequently, these multi-microfiber electrodes will present improved bioelectrochemical performance, such as higher current densities and lower onset potentials, which are beneficial when designing a high-performance biofuel cell. We acknowledge that our results apply only, in particular, to the enzyme immobilization method employed, and that designing more suitable immobilization strategies could culminate in the development of high performance biomicroelectrodes. However, we highlight that the straightforward nature of the chosen method involving simple steps such as incubation, drop-casting, and drying, is beneficial from a scalability point-of-view, as these steps are easy to integrate into mass production. These reasons explain our choice when producing these bioelectrodes.

To further corroborate our hypothesis that the s-FCF/ADH/Nafion electrode performs inferiorly to its counterparts, we performed a kinetic study by employing the Michaelis–Menten formalism. Here, we would like to emphasize that cyclic voltammetry was employed due to the small dimensions and brittleness of s-FCF/ADH/Nafion, as the electrolyte flow in convective measurements, such as chronoamperometry, leads to excessively noisy data and breakage of the microelectrode over time. Fig. 6a shows CVs of s-FCF/ADH/Nafion in increasing ethanol concentrations and indicates that the current response of this biomicroelectrode increases with ethanol concentration, plateauing at concentrations higher than 34 mmol L^{-1}. Indeed, the saturation concentration of s-FCF/ADH/Nafion is approximately 44 times lower than that observed for FCF/ADH/Nafion in a previous study.[23] The Lineweaver–Burk plot for s-FCF/ADH/Nafion (Fig. 6b) reveals a K_M^{app} of 95 mmol L^{-1}, nearly 450 times higher than that of FCF/ADH/Nafion (0.21 mmol L^{-1}).[23] The elevated K_M^{app} value for the s-FCF/ADH/Nafion electrode implies a substantially lower affinity for ethanol, suggesting that enzyme immobilization on the s-FCF/ADH/Nafion electrode is less effective. In all, the kinetic study highlights a significant limitation in enzyme attachment within microelectrode architectures, where restricted surface area and insufficient anchoring points may hinder optimal enzyme loading and orientation. Consequently, the diminished bioelectrochemical performance, as reflected in both SEM and cyclic voltammetry data, indicates that traditional immobilization techniques may not be sufficient for micro-scale bioelectrodes.

4 Discussion

The comparison between FCF, $\frac{1}{2}$FCF, and $\frac{1}{4}$FCF electrodes demonstrated that reducing the carbon material's mass does not significantly affect the current density or onset potential for

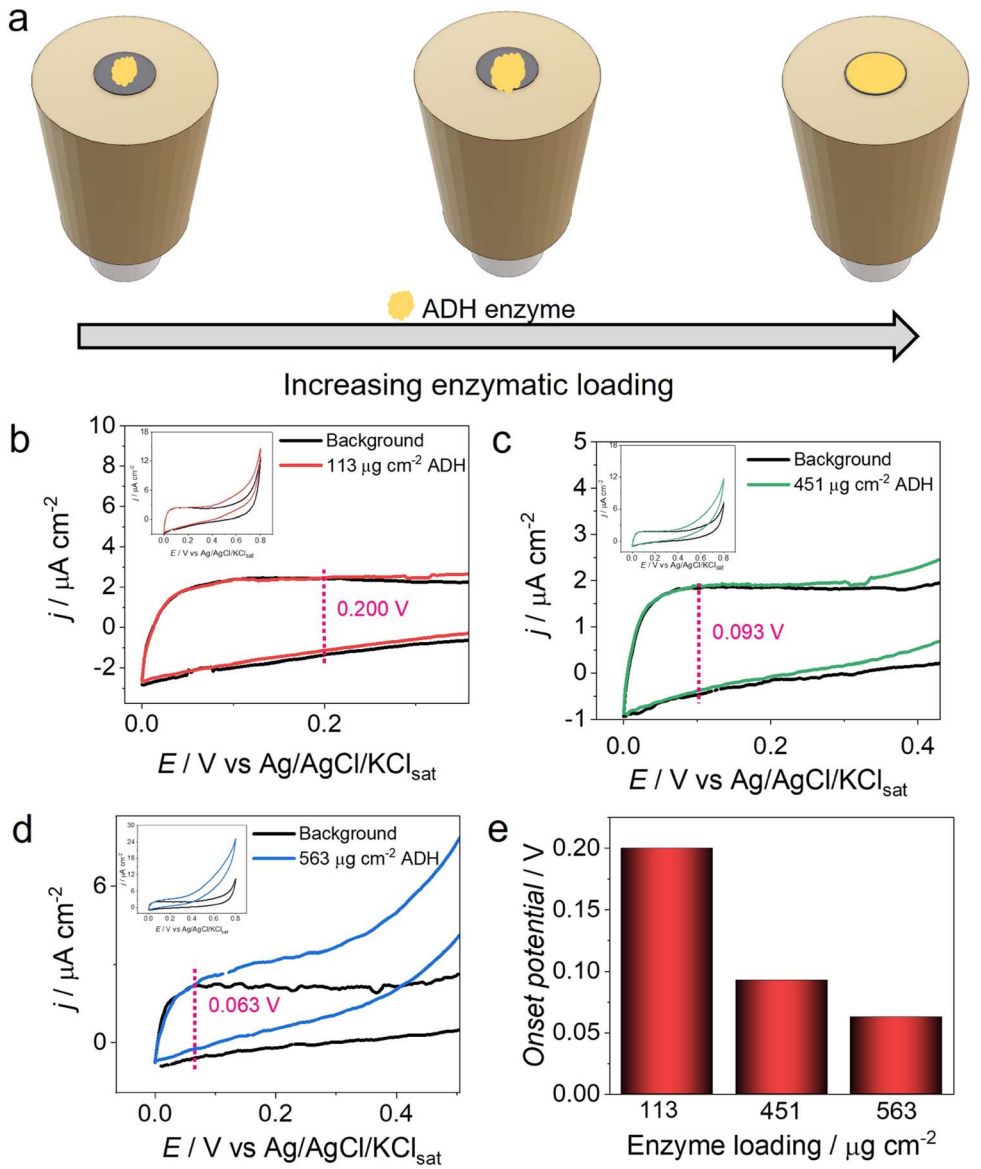

Fig. 5 (a) Schematic representation of ADH immobilization on the partially covered surface of a glassy carbon electrode. CVs of the GCE/ADH/Nafion bioelectrode with enzyme loadings of (b) 113 μg cm^{-2}, (c) 451 μg cm^{-2}, and (d) 563 μg cm^{-2}. (e) Comparison of the onset potential for ethanol bioelectrooxidation across GCE/ADH/Nafion bioelectrodes with varying enzyme loadings.

ethanol oxidation. These findings suggest that gravimetric miniaturization is a viable strategy for producing smaller-scale electrodes without compromising bioelectrochemical performance. The consistency across these electrodes can be attributed to their semi-infinite diffusion profile, as evidenced by the cyclic voltammograms with distinct oxidation and reduction peaks, characteristic of larger electrodes with planar diffusion. Thus, miniaturization in multi-fiber FCF electrodes does not significantly impact the diffusion profile or the ADH bioelectrochemical performance.

In contrast, the s-FCF electrode exhibited a distinct behavior. The CV of this electrode showed a sigmoidal shape with a steady-state current, indicative of radial diffusion, typical of microelectrodes. This behavior is expected for small-scale electrodes and, in theory, should offer greater efficiency in transporting active species to the electrode–electrolyte interface. However, the s-FCF/ADH/Nafion electrode showed inferior performance compared to the larger-scale bioelectrodes. This result was unexpected, as radial diffusion generally favors higher current densities. We hypothesize that this reduced performance is due to suboptimal enzyme immobilization on the electrode surface, as evidenced by the shift in onset potential to more positive values. This shift of approximately 100 mV suggests a significantly higher energy requirement for ethanol bioelectrooxidation, directly correlating with the efficiency of enzyme immobilization.

The results from the GCE with varying enzyme loadings support the hypothesis that low enzyme coverage can induce an onset potential shift. We observed that, as enzyme loading on the GCE surface decreased, the onset potential for ethanol

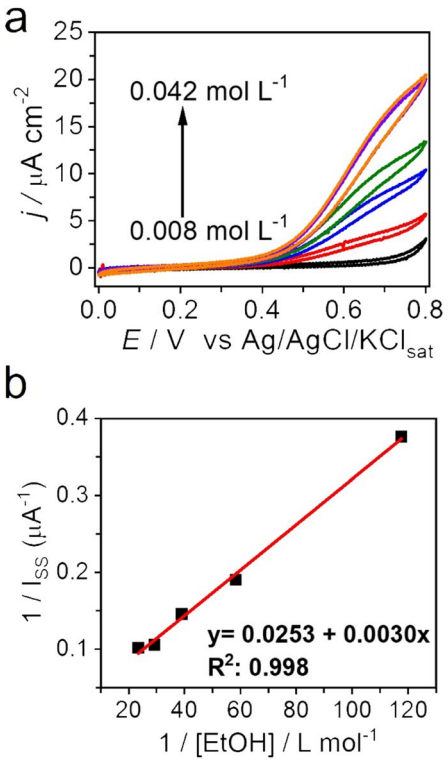

Fig. 6 (a) CVs of the s-FCF/ADH/Nafion bioelectrode recorded in the absence and presence of increasing ethanol concentrations, ranging from 8 mmol L^{-1} to 42 mmol L^{-1}. (b) Lineweaver–Burk plot derived from the current at 0.6 V, extracted from each CV shown in (a), to assess the kinetics of ethanol bioelectrooxidation.

oxidation increased, reinforcing the relationship between the amount of immobilized enzyme and the electrode's catalytic efficiency. Although the GCE with high enzyme coverage showed an onset potential only slightly higher than that of FCF/ADH/Nafion, the disparity in performance between s-FCF and larger-scale electrodes indicates a limitation of the immobilization method in microstructured electrodes.

The kinetic analysis using the Michaelis–Menten model provides a quantitative understanding of the bioelectrochemical performance of the electrodes. Both Lineaweaver–Burk (Fig. 6b) and Michaelis–Menten (Fig. S7) formalisms give a significantly higher K_M^{app} value for s-FCF/ADH/Nafion compared to FCF/ADH/Nafion indicating a lower affinity of the bioelectrode for ethanol bioelectrooxidation. These results support the hypothesis of low enzyme coverage and consequent reduced performance and emphasize the importance of developing new immobilization methodologies that promote more robust enzyme attachment on microstructures, such as the carbon microfiber used in s-FCF. While multi-fiber FCF electrodes retain desirable bioelectrochemical performance even with mass reduction, single-fiber microelectrodes require more specialized enzyme immobilization strategies to achieve the expected catalytic efficiency. Implementing advanced immobilization techniques to increase the density of enzymes effectively coupled to the electrode is therefore essential to enable the use of microstructures in high-performance bioelectrochemical devices. These insights are crucial for advancing miniaturized bioelectrodes and enhancing the integration of bioelectronic systems with sustainable, low-impact energy sources.

5 Conclusions

The findings of this study show the substantial impact of enzyme immobilization strategies on the bioelectrochemical efficiency of microelectrodes, particularly within systems employing single carbon microfibers. The pronounced shift in onset potential and the reduction in catalytic current density observed in single-fiber configurations indicate kinetic limitations likely resulting from suboptimal enzyme attachment and low electron transfer efficiency. These results suggest that conventional immobilization techniques, effective for macroscale electrodes, are insufficient to support efficient bioelectrocatalysis at micro-scale dimensions. To address these limitations, future studies should focus on the development of specialized immobilization methodologies tailored for microelectrode architectures. Advanced techniques such as covalent bonding, enzyme orientation control, and surface functionalization with conductive nanostructures may enhance enzyme loading density, stability, and electron transfer at the microelectrode interface. Additionally, employing hybrid materials and 3D-structured supports could further optimize enzyme–electrode coupling, facilitating higher catalytic activity and reduced overpotentials. Implementing these refined attachment approaches is essential for achieving high-performance, miniaturized bioelectrodes that meet the operational demands of biofuel cells and other bioelectronic applications in wearable and implantable devices.

Author contributions

Thiago Bertaglia: conceptualization, data curation, formal analysis, investigation, methodology, visualization, writing – original draft, writing – review and editing; Daniel S. de Sousa: conceptualization, investigation, formal analysis, methodology, visualization; Rafael N. P. Colombo: data curation, formal analysis, investigation, methodology, visualization, writing – original draft, writing – review and editing; Kamila C. Pagnoncelli: investigation, formal analysis, supervision; Rodrigo M. Iost: formal analysis, visualization, writing – original draft, writing – review and editing; Luana C. I. Faria: investigation, writing – review and editing; Graziela C. Sedenho: writing – review and editing; Frank N. Crespilho: conceptualization, funding acquisition, project administration, supervision, writing – original draft, writing – review and editing.

Conflicts of interest

There are no conflicts to declare.

Data availability

I, Frank N. Crespilho, acting as corresponding author of the work entitled "Single-fiber *versus* macroscale electrodes: enzyme loading and impacts on bioelectronic applications in flexible biodevices", and, on behalf of all co-authors, declare that the data regarding this work will be available upon reasonable request to the authors.

Supplementary information (SI): complementary electrochemical and SEM data, enzyme-loading measurements by UV-Vis, and the Michaelis–Menten curve. See DOI: https://doi.org/10.1039/d5ay01514f.

Acknowledgements

The authors acknowledge The São Paulo Research Foundation (FAPESP), the National Council for Scientific and Technological Development (CNPq) and the Coordination for the Improvement of Higher Education Personnel (CAPES) for the financial support. F. N. C acknowledges FAPESP for the grants 2018/22214-6, 2020/12404-2, 2022/09164-5, 2023/01529-7, 2022/06563-6, CAPES-MeDiCo 88881.504532/2020-01, CAPES 88887.513539/2020-00, and CNPQ 151837/2022-8. T. B., D. S. S, R. N. P. C., R. M. I., L. C. I. F, and G. C. S. acknowledge FAPESP for the fellowships 2016/08711-1, 2020/03681-2, 2023/08260-3, 2019/03033-3, 2021/05665-7, 2023/10667-4, 2019/21089-6, and 2020/04796-8.

References

1 F. Zhang, K. Yang, Z. Pei, Y. Wu, S. Sang, Q. Zhang and H. Jiao, *RSC Adv.*, 2022, **12**, 2391–2398.
2 G. Shang, D. Dinh, T. Mercer, S. Yan, S. Wang, B. Malaei, J. Luo, S. Lu and C.-J. Zhong, *ACS Sens.*, 2023, **8**, 1328–1338.
3 A. Kumar, R. K. Rakesh Kumar, M. O. Shaikh, C.-H. Lu, J.-Y. Yang, H.-L. Chang and C.-H. Chuang, *ACS Appl. Mater. Interfaces*, 2022, **14**, 55402–55413.
4 N. Promphet, C. Thanawattano, C. Buekban, T. Laochai, P. Rattanawaleedirojn, K. Siralertmukul, P. Potiyaraj, J. P. Hinestroza and N. Rodthongkum, *Adv. Mater. Technol.*, 2022, **7**, 2101684.
5 X. Xuan, C. Chen, A. Molinero-Fernandez, E. Ekelund, D. Cardinale, M. Swarén, L. Wedholm, M. Cuartero and G. A. Crespo, *ACS Sens.*, 2023, **8**, 2401–2409.
6 J. Wang, L. Wang, G. Li, D. Yan, C. Liu, T. Xu and X. Zhang, *ACS Sens.*, 2022, **7**, 3102–3107.
7 D. Sandil, S. C. Sharma and N. K. Puri, *J. Mater. Res.*, 2019, **34**, 1331–1340.
8 M. L. Yola and N. Atar, *Biosens. Bioelectron.*, 2019, **126**, 418–424.
9 R. A. S. Luz, A. R. Pereira, J. C. P. de Souza, F. C. P. F. Sales and F. N. Crespilho, *ChemElectroChem*, 2014, **1**, 1751–1777.
10 M. Sun, Y. Gu, X. Pei, J. Wang, J. Liu, C. Ma, J. Bai and M. Zhou, *Nano Energy*, 2021, **86**, 106061.
11 S. Yin, X. Liu, T. Kaji, Y. Nishina and T. Miyake, *Biosens. Bioelectron.*, 2021, **179**, 113107.
12 X. Huang, H. Li, J. Li, L. Huang, K. Yao, C. K. Yiu, Y. Liu, T. H. Wong, D. Li, M. Wu, Y. Huang, Z. Gao, J. Zhou, Y. Gao, J. Li, Y. Jiao, R. Shi, B. Zhang, B. Hu, Q. Guo, E. Song, R. Ye and X. Yu, *Nano Lett.*, 2022, **22**, 3447–3456.
13 J. Zhou, C. Liu, H. Yu, N. Tang and C. Lei, *Appl. Sci.*, 2023, 5917.
14 J. L. Zhang, Y. H. Wang, K. Huang, K. J. Huang, H. Jiang and X. M. Wang, *Nano Energy*, 2021, **84**, 105853.
15 Y. Zhang, H. Deng, Y. Zheng, X. Zheng, Z. He, C. Li, Z. Li, Z. Liu, Y. Zhu, L. Chen and G. Li, *ACS Appl. Nano Mater.*, 2024, **7**, 16466–16474.
16 Z. Chen, Y. Yao, T. Lv, Y. Yang, Y. Liu and T. Chen, *Nano Lett.*, 2022, **22**, 196–202.
17 I. Shitanda, K. Takamatsu, A. Niiyama, T. Mikawa, Y. Hoshi, M. Itagaki and S. Tsujimura, *J. Power Sources*, 2019, **436**, 226884.
18 F. C. P. F. Sales, R. M. Iost, M. V. A. Martins, M. C. Almeida and F. N. Crespilho, *Lab Chip*, 2013, **13**, 468–474.
19 R. M. Iost, F. C. P. F. Sales, M. V. A. Martins, M. C. Almeida and F. N. Crespilho, *ChemElectroChem*, 2015, **2**, 518–521.
20 N. Lalaoui, A. De Poulpiquet, R. Haddad, A. Le Goff, M. Holzinger, S. Gounel, M. Mermoux, P. Infossi, N. Mano, E. Lojou and S. Cosnier, *Chem. Commun.*, 2015, **51**, 7447–7450.
21 S. Tvorynska, J. Barek and B. Josypcuk, *Bioelectrochemistry*, 2022, **148**, 108223.
22 A. S. Campbell, Y. J. Jeong, S. M. Geier, R. R. Koepsel, A. J. Russell and M. F. Islam, *ACS Appl. Mater. Interfaces*, 2015, **7**, 4056–4065.
23 G. C. Sedenho, I. T. Neckel, R. N. P. Colombo, J. C. Pacheco, T. Bertaglia and F. N. Crespilho, *Adv. Energy Mater.*, 2022, **12**, 2202485.
24 V. Davis, N. Heidary, A. Guiet, K. H. Ly, M. Zerball, C. Schulz, N. Michael, R. von Klitzing, P. Hildebrandt, S. Frielingsdorf, O. Lenz, I. Zebger and A. Fischer, *ACS Catal.*, 2023, **13**, 6312–6327.
25 M. A. Oke, S. A. Ojo, S. A. Fasiku and E. A. Adebayo, *Nanotechnology*, 2023, **34**, 385101.
26 M. Tawalbeh, R. Muhammad Nauman Javed, A. Al-Othman and F. Almomani, *Fuel*, 2022, **322**, 124237.
27 A. R. Pereira, J. C. P. De Souza, A. D. Gonçalves, K. C. Pagnoncelli and F. N. Crespilho, *J. Braz. Chem. Soc.*, 2017, **28**, 1698–1707.
28 M. A. Ali, G. C. Sedenho, J. C. Pacheco, R. M. Iost, A. Rahman, A. Hassan, D. R. Cardoso, R. S. Gomes and F. N. Crespilho, *J. Power Sources*, 2022, **551**, 232164.
29 A. R. Pereira, J. C. P. de Souza, R. M. Iost, F. C. P. F. Sales and F. N. Crespilho, *J. Electroanal. Chem.*, 2016, **780**, 396–406.
30 M. A. Ali, A. Hassan, G. C. Sedenho, R. V. Gonçalves, D. R. Cardoso and F. N. Crespilho, *J. Phys. Chem. C*, 2019, **123**, 16058–16064.
31 K. C. Pagnoncelli, A. R. Pereira, G. C. Sedenho, T. Bertaglia and F. N. Crespilho, *Bioelectrochemistry*, 2018, **122**, 11–25.
32 A. R. Pereira, R. A. S. Luz, F. C. D. A. Lima and F. N. Crespilho, *ACS Catal.*, 2017, **7**, 3082–3088.
33 S. Q. Nascimento, R. M. Iost, T. C. Oliveira, R. N. Colombo, L. C. I. Faria, T. Bertaglia, J. C. Pacheco, M. N. Oliveira,

E. R. Manuli, G. M. Pereira, E. C. Sabino and F. N. Crespilho, *Biosens. Bioelectron.: X*, 2024, **18**, 100472.
34 J. C. P. de Souza, W. O. Silva, F. H. B. Lima and F. N. Crespilho, *Chem. Commun.*, 2017, **53**, 8400–8402.
35 H. M. Man, I. Mazurenko, H. Le Guenno, L. Bouffier, E. Lojou and A. De Poulpiquet, *Anal. Chem.*, 2022, **94**, 15604–15612.
36 F. Conzuelo, N. Marković, A. Ruff and W. Schuhmann, *Angew. Chem., Int. Ed.*, 2018, **57**, 13681–13685.